



# Modeling the Influence of the Interfacial Zone on the DC Electrical Conductivity of Mortar

E.J. Garboczi, L.M. Schwartz, and D.P. Bentz  
National Institute of Standards and Technology, Building Materials Division,  
Gaithersburg, Maryland

*The interfacial zone separating cement paste and aggregate in mortar and concrete is believed to influence many of the properties of these composites. The available experimental evidence, obtained on artificial geometries, indicates that the DC electrical conductivity of the interfacial zone, because of its higher porosity, may be considerably larger than that of the bulk cement paste matrix. This paper presents the theoretical framework for quantitatively understanding the influence of the interfacial zone on the overall electrical conductivity of mortar, based on realistic random aggregate geometries. This understanding is also used, via an electrical analogy with Darcy's law, to make predictions about the effect of the interfacial zone on fluid permeability. The results obtained for mortar should also pertain to concrete.* ADVANCED CEMENT BASED MATERIALS 1995, 2, 169–181

**KEY WORDS:** Aggregate, Concrete, Electrical conductivity, Interfacial zone, Model, Mortar, Percolation, Permeability

**T**he DC electrical conductivity of mortar and concrete is important both as a means of probing the structure of these materials and as a measure of ionic diffusivity [1], via the Nernst-Einstein relation [2]. Diffusivity is of interest in connection with a range of issues related to durability, such as sulfate attack and chloride ion-induced corrosion of steel reinforcing bars [3].

Concrete conducts electricity because of its porous cement paste matrix, which is a conductor when saturated with the electrolytic pore fluid [4–6]. Much recent work has been done on understanding how the microstructure of cement paste determines its electrical conductivity [4,5,7–9]. However, relatively little work has been done on how the conductivity of concrete de-

pends on quantities like the number and arrangement of aggregate particles and on the cement paste-aggregate interfacial zone [6,10]. This is at least partly due to the complicated random structure of concretes and mortars. Experimentally, some synthetic aggregate:cement paste geometries have been investigated [11,12] that did not, however, take into account the random geometry and topology of the real material phases.

Concrete is a random composite material at many length scales [13], from the nanometer length scale of the C-S-H structure in the cement paste matrix, to the micrometer length scale of the unhydrated cement grains and larger capillary pores, and finally up to the millimeter and centimeter length scale of the aggregate particles used in a typical concrete. Accordingly, it is not practical to try to predict the electrical properties from the material structure while simultaneously considering all these length scales. Instead, one must focus on a given length scale and describe the microstructure and properties in mathematical language appropriate to this length scale. In this paper, we are concerned with the (approximately 10–1000  $\mu\text{m}$ ) length scale that adequately describes a typical mortar [14,15]. Within this framework, mortar (and concrete) can be approximately viewed as a three-phase composite [16–18] of bulk cement paste, aggregate, and interfacial zone cement paste (see Figure 1), where all three phases can be thought of as uniform continuum materials. In a mortar, the aggregate particles typically range in size from 100  $\mu\text{m}$  to a few millimeters. Interfacial zones are significantly smaller, on the order of 10–50  $\mu\text{m}$  in thickness [19,20]. Typical volume fractions occupied by the aggregate particles in mortars are about 50%, with the remaining volume comprised of bulk and interfacial zone cement paste. Aggregate volume fractions are usually somewhat higher in concrete, on the order of 60% [14].

In a three-phase composite model, the volume frac-

Address correspondence to: Edward Garboczi, National Institute of Standards and Technology, Building Materials Division, Building 226, Room B348, Gaithersburg, MD 20899-001.

Received October, 21, 1994; Accepted February 14, 1995

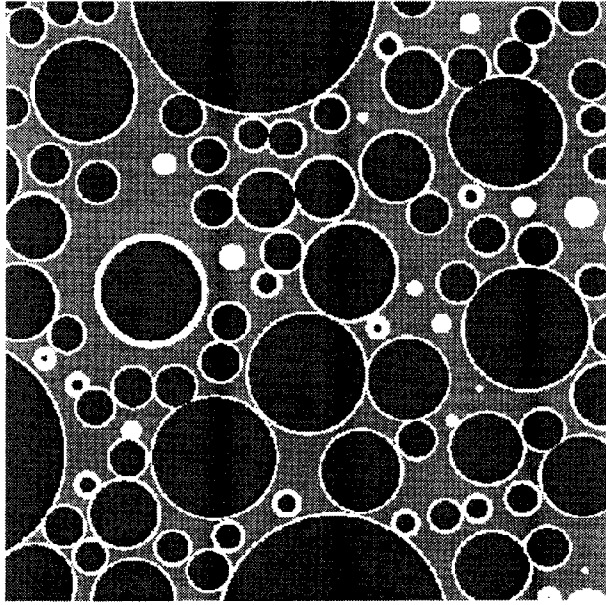


**FIGURE 1.** The structure of mortar, as represented by the random aggregate model. There are four sizes of sand grains with diameters (in  $\mu\text{m}$ ) of 1,500, 750, 500 (dark gray), and 250. The thickness of the interfacial zone region (white) is 20  $\mu\text{m}$ . The bulk matrix cement paste is shown in light gray. The total volume fraction of sand is 54%, with the sand size distribution as given in Table 1.

tion assigned to the interfacial zone phase depends on what thickness is taken to define the boundary between the interfacial zone and the bulk cement paste. Figure 2 shows, using a recently developed model for the structure of mortar [15], how the volume fraction of cement paste belonging to the interfacial zone phase

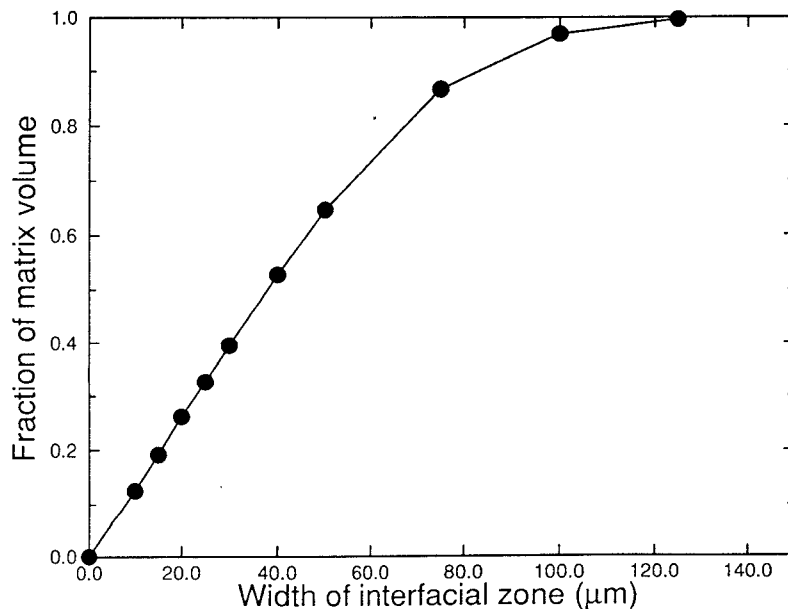


**FIGURE 2.** For size distribution of sand grains determined experimentally [15], the fraction of the total cement paste volume occupied by the interfacial zone cement paste is shown as a function of the interfacial zone thickness. (Here the grains are assumed to be spherical.)

varies as a function of this assumed thickness. In this model, sand grains are taken to be spherical with a realistic size distribution [15]. The interfacial zones are viewed as uniform thickness shells placed concentrically around each aggregate or sand grain. Because the average particle size of the cement is much smaller than the average particle size of the sand, the thickness of the interfacial zone is determined by the cement particle size. This thickness then has the same value for each sand grain [21]. Figure 2 clearly shows that, for values of the interfacial zone thickness around 20  $\mu\text{m}$ , the interfacial zone cement paste occupies 20 to 30% of the total cement paste volume, and therefore 10 to 15% of the total mortar volume. Because the interfacial zone cement paste occupies a significant volume fraction, the physical properties of this phase will certainly have an influence on the overall behavior of the mortar/concrete composite [22,23]. This would be true even if this phase were discontinuous. However, recent modeling and mercury injection experimental work showed that, even if the interfacial zone thickness is taken to be as small as 10  $\mu\text{m}$ , the interfacial zone cement paste phase can still form a continuous percolating channel, which implies an even larger effect on the transport properties of the composite [15,24].

Most real mortars and concretes have entrapped or entrained air voids. If air voids are present (and remain filled with air rather than pore fluid), they can be treated as an insulating "aggregate" particle with an interfacial zone probably similar to that surrounding the usual aggregate particles [25]. We will not consider air voids in the rest of this paper.

## Constituent Properties in the Three-Phase Model

For the purposes of electrical conduction, the aggregate grains are simply inert obstacles to the flow of current. The basic model is then defined by two parameters: (1) the structure of the interfacial layer, and (2) the electrical contrast between this layer and the bulk cement paste. Clearly, both parameters will depend on the water:cement ratio as well as other properties of the bulk paste.

It is well-known that the aggregate-cement paste interfacial zone consists of a region up to approximately 50  $\mu\text{m}$  thick around each aggregate grain. Within this zone, there is higher porosity, larger pores, and a higher volume fraction of calcium hydroxide [19,20]. This is the case for aggregate that is much less porous than the cement paste, like quartz or granite. In the case of lightweight aggregate, like a porous limestone, or aggregate that can react with water, like cement clinker aggregate, this situation can be reversed with the interfacial zone actually denser than the bulk cement paste [21,26]. This paper concentrates on the case where the interfacial zone is less dense than the bulk cement paste, although the same models can also handle the case of denser interfacial zones.

In porous materials in general and cement paste in particular, the conductivity increases roughly as a power of the porosity. This behavior occurs when the pore space is filled with a conductive material, which is pore fluid in cement paste. The exponent in this power law generally lies between 1 and 3 and is, in many cases, quite close to the value 2 [27].

Figure 3 shows schematically how the capillary porosity varies, and therefore how the conductivity might vary, across the interfacial zone by assuming that the conductivity is proportional to the square of the porosity. In this paper, we replace the variable conductivity interfacial zone region with a shell of fixed width and constant conductivity, for the sake of simplicity. There is more than one way to carry this out. We choose to average the conductivity by integrating across the interfacial zone, and then assume a fixed width shell around each aggregate grain in which the conductivity  $\sigma_s$  is higher than that of the bulk cement paste and is defined by:

$$\sigma_s \equiv \frac{\int_0^h \sigma(x) dx}{h} \quad (1)$$

where  $h$  is the assumed thickness of the interfacial zone in which the extra conductivity is concentrated and  $\sigma(x)$  is the actual conductivity as a function of  $x$ , the distance from the aggregate surface, as schematically shown in Figure 3. All the other cement paste outside of the shell of thickness  $h$  is given the bulk cement paste value of conductivity,  $\sigma_p$ . For the schematic data shown in Figure 3, the ratio  $\sigma(x=0)/\sigma_p$  is about 14. Using  $h = 10, 20,$  and  $30 \mu\text{m}$ , in combination with eq 1, the value of  $\sigma_s/\sigma_p$  is calculated to be 8, 5, and 4; respectively. This procedure has the advantage of forcing the chosen interfacial zone conductivity to be smaller as the width of the zone is made larger, so that the current around each grain should remain approx-

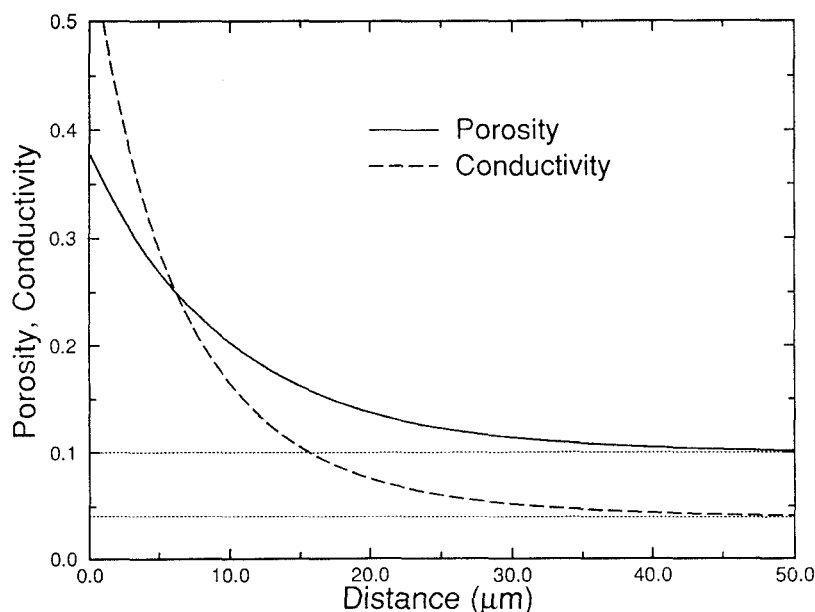


**FIGURE 3.** Schematic representation of how the capillary porosity and conductivity may vary across the interfacial zone. The horizontal dotted lines show the bulk cement paste values for both quantities.

imately fixed and not depend sensitively on the assumed value of  $h$ .

Several authors have carried out experiments with planar or cylindrical aggregate shapes, so that the bulk cement paste and interfacial zone electrical flow paths are both one-dimensional and in parallel. In this simple geometry, separate measurements of the bulk cement paste conductivity and the composite conductivity can be combined to extract a value for  $\sigma_s/\sigma_p$ , if a value for  $h$  is assumed. A range of values has been found, from about 10 [11], assuming  $h = 20 \mu\text{m}$ , to 12–15 [12], assuming  $h = 100 \mu\text{m}$ . This latter value for  $h$  seems much too large, since scanning electron microscopy investigations of the interfacial zone generally find that the porosity of the interfacial zone decreases to the bulk cement paste value by a distance of 30–50  $\mu\text{m}$  from the aggregate grain surface [19,20].

Assuming a fixed thickness for the interfacial zone region, it is possible to compute separate values of porosity for this effective interfacial zone and for the bulk cement paste. Bourdette et al. have done this for two different mortars, 0.4 water:cement ratio (w:c) and 0.5 w:c, with slightly varying size distributions and amounts of sand, both between 50 and 60% by volume [28]. They find values of the interfacial zone (bulk cement paste) porosity, ranging from 46% (22%) to 30% (21%), for an assumed value of  $h = 30 \mu\text{m}$ . Using the conductivity versus capillary porosity curve for cement paste established in earlier computational work [4], Bourdette et al. found that these pairs of porosities correspond to ratios of conductivities ranging from  $\sigma_s/\sigma_p = 6$ –15, in reasonable agreement with the experimental values and with the simple schematic data shown in Figure 3. We note that the theoretical relation for bulk cement paste conductivity derived earlier [4] is, for capillary porosities larger than 18%, essentially quadratic in the capillary porosity, in agreement with the general ideas discussed previously and displayed in Figure 3.

Because there is no definitive value established experimentally for the value of  $\sigma_s/\sigma_p$ , we have chosen to allow this parameter to vary in the following computations and have studied the dependence of the composite conductivity for a given sand content on the value of  $\sigma_s/\sigma_p$ . However, based on the mercury intrusion and modeling results for ref 15, we have chosen  $h = 20 \mu\text{m}$  as the best value for the width of the interfacial zone. We emphasize that extracting the value of  $\sigma_s/\sigma_p$  from experiments will require an assumption for the value of  $h$ . That is another reason to investigate the composite conductivity as a function of a variable interfacial zone conductivity.

Although the model we pursue in the remainder of this paper is highly simplified, we emphasize that its essential features could be specified in detail if more

experimental data on the structure of mortars were available. In particular, we feel that nuclear magnetic resonance (NMR) studies would be of great value in determining the model's parameters. NMR may be particularly useful, because the larger pores in the interfacial zone could be seen in relaxation studies as an independent contribution to the pore size distribution [29,30]. By contrast, in mercury intrusion the interfacial zone pores are detected at their correct size only if this zone percolates through the material. Before they are percolated, they will be classified as smaller bulk cement paste pores [15]. Such experiments could also fix the relative weights of the interfacial zone and bulk cement paste porosities, thereby constraining the thickness of the layer and thus the electrical contrast. In principle, similar information is available directly from microscopy, but NMR has the advantage of being a nondestructive, noninvasive measurement.

## Periodic and Random Models for Mortar

The random arrangement of multisized aggregate particles in real mortar or concrete plays an important role in determining the effective properties of the composite. However, ordered periodic arrangements of aggregate grains are easier to handle computationally. Although they cannot be quantitatively accurate, results obtained from periodic models can still give qualitative insight, as aggregate-aggregate interactions and interfacial zone overlap do play an important role.

The periodic model that is investigated in this paper is a body-centered cubic (BCC) [31] arrangement of spherical sand grains, chosen to have a diameter of 400  $\mu\text{m}$  and an interfacial zone thickness of  $h = 20 \mu\text{m}$ . The value of 400  $\mu\text{m}$  was chosen from the sand particle size distribution used in ref 15 as being a compromise between the number fraction-weighted and volume fraction-weighted average particle diameters. The size of the unit cell was chosen so that the interfacial zones would be percolated and so that the sand volume fraction was 54%, with the interfacial zone occupying approximately one-third of the total paste volume fraction of 46%. This choice of parameters produces a system in rough agreement with the model studied in ref 15. A slice through the body diagonal of the cubic unit cell is shown in Figure 4, with the three phases shown in different gray levels. By convention  $\sigma_p = 1$ , while the value of  $\sigma_s/\sigma_p$  was allowed to vary freely.

To compute the overall conductivity of this periodic composite, a cubic unit cell containing two sand grains was digitized into a three-dimensional array of pixels, typically  $128 \times 128 \times 128$ . A macroscopic electric field was applied in one of the principal cubic directions.

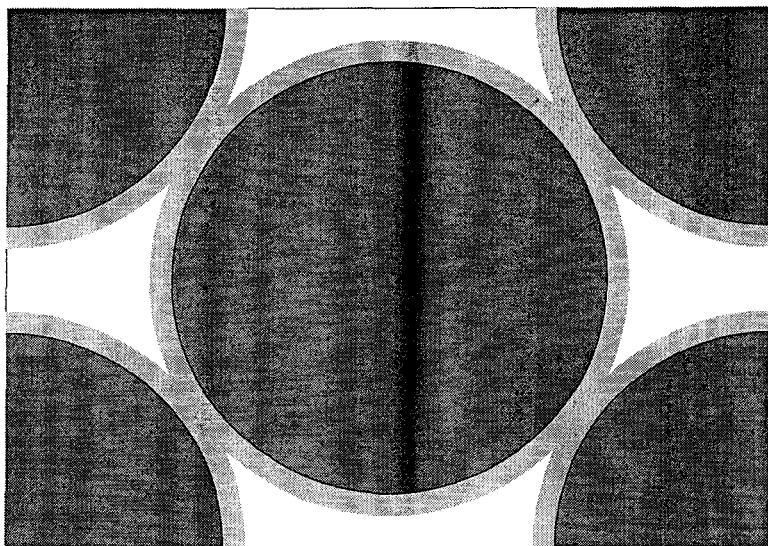


**FIGURE 4.** Cross-sectional view (taken through the cubic unit cell body diagonal) of the body-centered cubic (BCC) packing of equal size spherical sand grains. The bulk cement paste is shown in white, the sand grains in dark gray, and the interfacial zone in light gray.

Each pixel was then treated as a tri-linear finite element, which resulted in a set of  $128^3$  linear equations that were solved with a conjugate gradient algorithm [32,33]. A resolution of  $64 \times 64 \times 64$  was also used, with only very small changes in overall results, so that the  $128^3$  resolution was judged to be adequate to represent both the sand grain and, more importantly, the thin interfacial zone volume.

To study a mortar with a more realistic random sand grain arrangement, we used the system studied in ref 15 and shown in Figure 1. From the experimentally measured sand grain size distribution used there, we chose four representative diameters: 250, 500, 750, and 1,500  $\mu\text{m}$ . In effect, we reduced the total number of particles needed in the model by eliminating the largest and smallest grain sizes. (The ratio of largest diameter to smallest diameter determines how many particles are required to achieve a statistically representative volume.) For the maximum sand grain volume fraction studied, a total of 6,500 particles was used.

The sand grains were randomly placed, largest first and smallest last, such that no sand grains overlapped. The center coordinates and radius of each sphere was recorded in a data list. Interfacial zones 20  $\mu\text{m}$  thick were added to each grain. The interfacial zone volume was determined by point counting [15], the aggregate volume was determined by just adding up the volumes of individual sand grains, and the bulk cement paste was the remaining volume.

The connectivity of the interfacial zone phase was computed using a burning algorithm [15]. Figure 5 shows the connectivity of the interfacial zone phase as a function of sand volume fraction. The y-axis, labeled "Fraction Connected," is just the fraction of the total interfacial zone volume at a given sand volume fraction that is part of a connected path across the sample. The

interfacial zone phase first becomes partially connected at a sand volume fraction of about 36%, and essentially all of the interfacial zones are connected to each other by a sand volume fraction of 51%.

The conductivity of the random sand grain mortar model was computed quite differently from that of the periodic model for the following reason. The largest unit cell we can presently use for electrical computations using the conjugate gradient/finite element method is actually around  $128^3$ . The size is dictated by the limitations of the computers to which we have access. This is not enough resolution to adequately represent more than a few grains and their associated interfacial zones. To compute the conductivity of statistically representative volumes of material containing thousands of sand grains requires a different approach.

Here we adopt a random walk algorithm, used extensively in studies of disordered porous media [34] and composite materials [35]. For a material where only one phase has a non-zero conductivity, the algorithm is especially simple. Random walkers are started at various positions in the conductive phase and allowed to take unit length steps in random directions at every time step. The mean square distance traveled by each walker is computed as a function of the number of time steps. If a projected step would take the walker into a nonconductive phase, then that step is not allowed, but the clock is still advanced one time step. Eventually, the mean-square distance versus the number of time steps is a straight line whose slope is the diffusion coefficient of the conductive phase. Multiplying by the volume fraction of the conducting phase then gives the overall conductivity of the composite, normalized by the conductivity of the pure conducting phase [34].

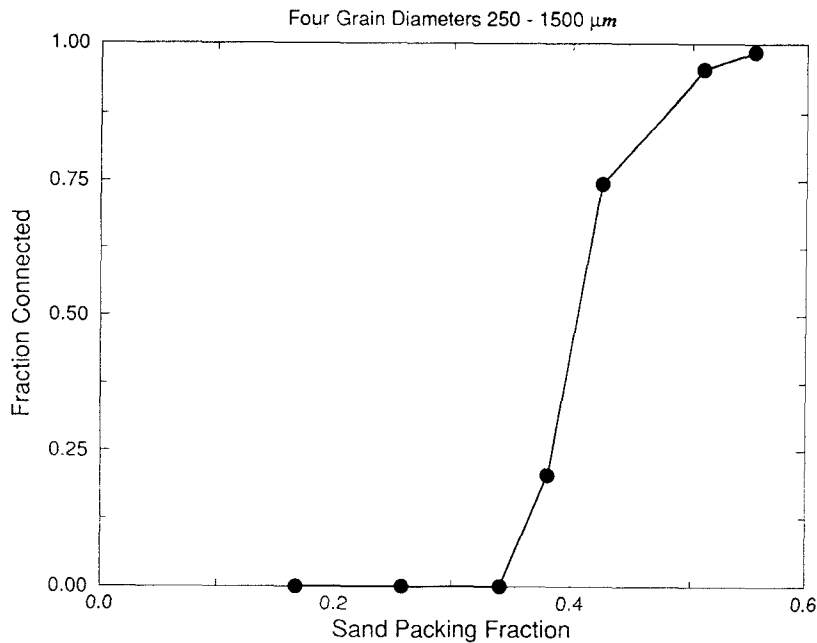


**FIGURE 5.** Percolation curve for random sand grain mortar model, for a 20  $\mu\text{m}$  thick interfacial zone. The x-axis is the sand volume fraction, and the y-axis is the fraction of the interfacial zone phase that is contained in the percolating cluster.

When two or more phases are conducting with different phase conductivities, then the algorithm is somewhat more complicated, although this case has also been studied by Hong et al. [36]. Basically, the step rate in a phase increases with conductivity of the phase. Additionally, the probability of stepping across a phase boundary from phase A to phase B is biased based on the relative conductivity of the two phases. Again the mean square displacement versus the number of time steps gives a diffusivity from which is derived the overall conductivity [37].

The random walk algorithm allows the sand grains and interfacial regions to be stored as geometrical objects rather than as collections of pixels, so that the resolution is essentially that of the step size used. This step size can be small compared to the interfacial zone thickness  $h$  without any increase in the computational storage required. This means that a large number of particles as well as the thin interfacial zones can be simultaneously resolved. Run times will increase as the step size decreases, however.

## Electrical Conductivity Results

We first present the results for the BCC periodic mortar model to display overall trends and to point out general behavior. Figure 6 shows, for the 54% sand volume BCC mortar model, the overall conductivity of the composite,  $\sigma$ , divided by the conductivity of the bulk cement paste matrix,  $\sigma_p$ . The x-axis is the ratio of the conductivity of the interfacial zone cement paste,  $\sigma_s$ , to  $\sigma_p$ . The interfacial zone cement paste is percolated in

this model and so plays a strong role in the overall conductivity as can be seen from the graph. Several points are worthy of note.

The conductivity at  $\sigma_s/\sigma_p = 1$  is that which would be obtained if the interfacial zone cement paste had the same porosity and therefore the same conductivity as the bulk cement paste. The presence of the insulating sand grains in this case reduces the overall normalized conductivity from 1 to 0.35. This is consistent with a 3/2 power law found in suspensions of spheres and in many porous rocks, where the normalized conductivity goes like the 3/2 power of the conductive phase volume fraction. In this case,  $(0.46)^{3/2} = 0.31$  [27,38,39].

The composite conductivity can be thought of as the result of a competition between the insulating sand grains, which tend to lower the overall conductivity, and the interfacial zone cement paste shells, which tend to raise the overall conductivity, when  $\sigma_s > \sigma_p$ . Figure 6 shows that when  $\sigma_s/\sigma_p \geq 6$ , the composite conductivity first achieves a value equal to the matrix conductivity; so for this microstructure, this value of  $\sigma_s/\sigma_p$  causes the greater interfacial zone conductivity to "cancel out" the effect of the zero conductivity sand grains. For values of  $\sigma_s/\sigma_p < 6$ , the overall conductivity is less than the bulk cement paste conductivity, whereas for  $\sigma_s/\sigma_p > 6$ , it is more. When  $\sigma_s/\sigma_p = 20$ , the highest value shown in the graph, the composite conductivity achieved is 2.6 times higher than the bulk cement conductivity.

The solid curve in Figure 6 is a Padé approximant [40] that has been employed [41] to describe the conductivity of porous sandstone rocks where the sand

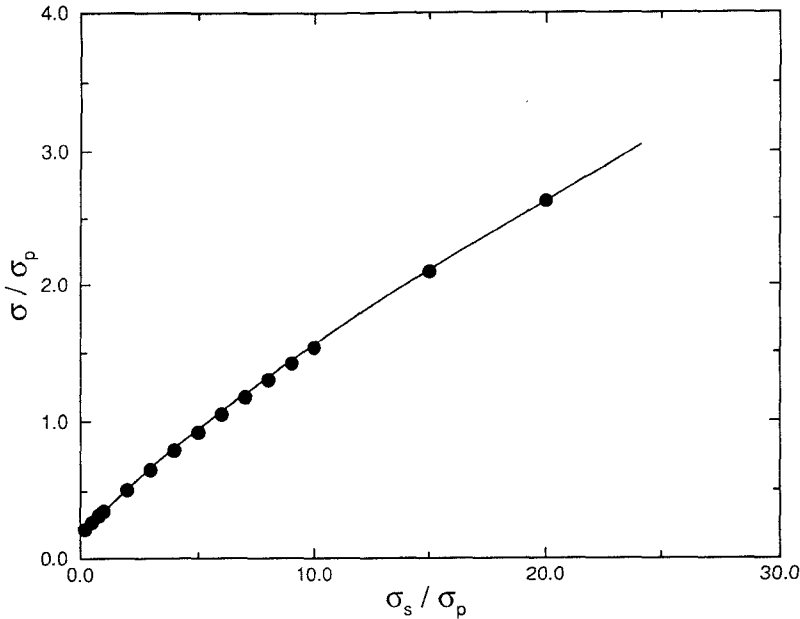


**FIGURE 6.** Composite conductivity for the body-centered cubic (BCC) model is plotted versus the interfacial zone conductivity. (Both are normalized by bulk paste conductivity.) The solid dots are the numerical data, and the solid line is the Padé approximant explained in the text.

grains have a thin clay coating that has a higher conductivity than the electrolytic pore fluid. This is a situation analogous to the mortar and concrete conductivity problem being studied here. The Padé approximant is a ratio of a quadratic polynomial to a linear polynomial,

$$\frac{\sigma}{\sigma_p} = \frac{b + cx + dx^2}{1 + ax} \quad (2)$$

where  $x = \sigma_s/\sigma_p$ . The parameters ( $a, b, c, d$ ) are given by combinations of four well-defined parameters ( $F, \Lambda, f, \lambda$ ), which are defined in terms of the following two limits of the curve shown in Figure 6 [41].

The first limit, in which the interfacial zone is only slightly more (or slightly less) conductive than the bulk cement paste matrix,  $\sigma_s/\sigma_p \rightarrow 1$ , is given exactly by perturbation theory as

$$\frac{\sigma}{\sigma_p} \cong \frac{1}{F} \left( 1 + \frac{2h(\sigma_s/\sigma_p - 1)}{\Lambda} \right) \quad (3)$$

where  $1/F$  is the ratio of the conductivity of the mortar to the conductivity of the bulk paste when  $\sigma_s/\sigma_p = 1$ , and  $\Lambda$  is a length parameter defined using the ratio of a volume integral to a surface integral of the electric fields obtained from the solution of the  $\sigma_s = \sigma_p$  problem [41]. When  $\sigma_s/\sigma_p = 1$ ,  $\sigma/\sigma_p = 1/F$ , and when  $\sigma_s/\sigma_p$  is close to 1, eq 3 is linear in  $\sigma_s/\sigma_p$  with a slope given by the ratio  $2h/(F\Lambda)$  [41].

The second limit is when the conductivity of the (assumed fully connected) interfacial zone is much larger than that of the bulk cement paste,  $\sigma_s/\sigma_p \gg 1$ . In

this limit, the composite conductivity is given exactly by perturbation theory as [41]

$$\frac{\sigma}{\sigma_p} \cong \frac{1}{f} [h(\sigma_s/\sigma_p - 1) + \lambda/2] \quad (4)$$

where  $1/f$  is the conductivity of the problem where  $\sigma_p = 0$  and  $\sigma_s = 1$ , and  $\lambda$  is another length parameter that comes from a ratio of a surface integral and a volume integral of the electric fields found in a solution of this same problem [41]. Fitting eq 2 to eqs 3 and 4 gives the four unknown coefficients ( $a, b, c, d$ ).

Clearly, the Padé approximant provides an excellent fit to the computed data points in Figure 6, so that this analytical curve could be used to accurately predict the composite conductivity at other values of  $\sigma_s/\sigma_p$  that were not numerically computed. The BCC periodic mortar model has served to illustrate some generic effects of the interfacial zone conductivity on the overall mortar conductivity. The random mortar model, which is expected to more faithfully describe the real material, is discussed next.

In Figure 7, we have the counterpart of Figure 6 for the random mortar model. As in Figure 6, the overall shape of the curve is concave down. The curve could at most be straight. This would be the case if the two phases, interfacial zone and bulk cement paste, were exactly in parallel. Then the overall conductivity would be given by a simple linear combination of the two phase conductivities, and as  $\sigma_s$  increased, the overall conductivity would increase linearly in this parameter. Because the microstructure is such that the two cement paste phases are not exactly in parallel, then the curve must be sublinear, or concave down. As  $\sigma_s/\sigma_p \rightarrow \infty$ , the curve will of course go to a straight line as in eq 4.

To achieve an overall conductivity that is equal to the bulk cement paste conductivity, the value of  $\sigma_s/\sigma_p$  must be equal to approximately 8, as can be seen in Figure 7. This is higher than in the BCC periodic model due to the greater tortuosity of the interfacial zone cement paste phase in the random model and its smaller volume fraction compared to the BCC model. Increasing  $\sigma_s/\sigma_p$  has therefore a somewhat lesser effect on the overall conductivity. At  $\sigma_s/\sigma_p = 20$ , the overall conductivity is about 1.8, which is also significantly less than in the BCC periodic mortar model, for the same reasons.

The solid line in Figure 7, is a Padé approximant similar to that in Figure 6. The fit is less good than in the BCC case, again an indication of the greater complexity of the random mortar model and of real mortars. However, the asymptotic slope of the Padé approximant for large values of  $\sigma_s/\sigma_p$  should be accurate, so that this curve can be safely extrapolated to predict the effect on  $\sigma/\sigma_p$  of much higher values of  $\sigma_s/\sigma_p$ .

As measurements of the conductivity of mortars (and the cement paste they are made from) become available, curves like those shown in Figure 7 will serve to identify the conductivity value for the interfacial zone that provides the best match to the composite conductivity. A second important experimental data set will be obtained by measuring the conductivity of a mortar as a function of sand volume fraction. One important aspect of such a data set is the dilute limit, where the sand volume fraction is low. The composite conductivity in this regime contains important information about the conductivity and size of the interfacial zone. This is the case because exact analytical cal-

culations can be made of the influence of a few sand grains surrounded by an interfacial zone shell placed in a matrix. For the composite to be considered to be in the dilute limit, the volume fraction of spherical inclusions must be small enough (<5%) so that particles can be considered individually and do not affect each other.

Consider mono-size spherical particles of conductivity  $\sigma_1$  and radius  $b$ , each surrounded by a concentric shell of thickness  $h$  and conductivity  $\sigma_2$ , and all embedded in a matrix of conductivity  $\sigma_3$ . The volume fraction of sand grains is  $c$ . Then  $\sigma/\sigma_3$ , the overall composite conductivity normalized by the matrix conductivity, is given by the expansion:

or

$$\frac{\sigma}{\sigma_p} = 1 + mc + O(c^2) \quad (6)$$

Equation 5 has been derived by exactly solving for the local electric fields and currents when the above physical system is placed in an (initially) uniform electric field. Appropriate current and field averages are then calculated to define the effective conductivity [42,43]. To make the connection to our mortar problem, let  $\sigma_1 = 0$ ,  $h =$  the interfacial zone thickness,  $\sigma_2 = \sigma_s$  (interfacial zone conductivity), and  $\sigma_3 = \sigma_p$  (bulk cement paste conductivity).

For the random mortar model, or indeed for a real mortar, there is a size distribution of sand grain radii  $b_i$ , while the value of  $h$  is fixed. That implies that the slope  $m_i$  for each kind of particle will be a function of  $b_i$ ,

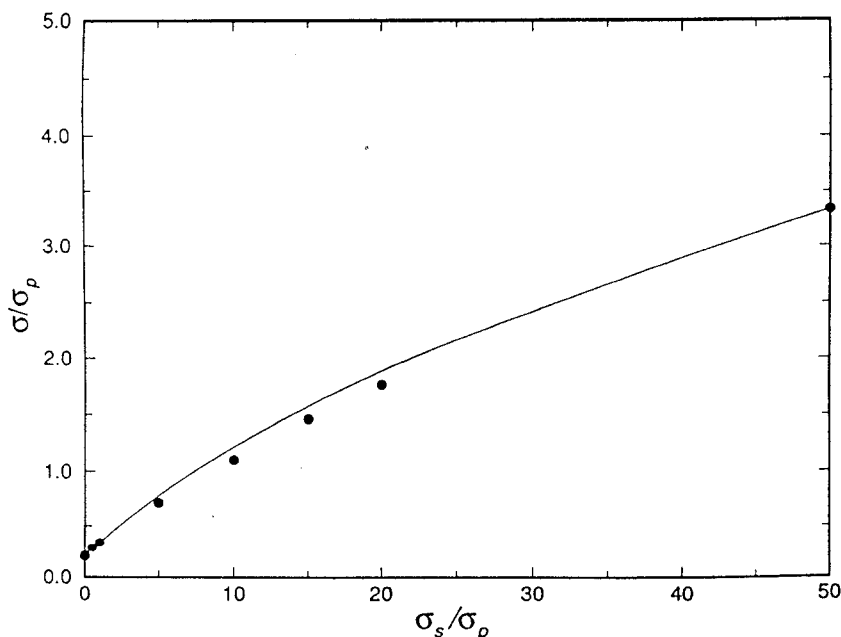


**FIGURE 7.** Composite conductivity for the random mortar model is plotted versus the interfacial zone conductivity. (Both are normalized by bulk paste conductivity.) The solid dots are the numerical data, and the solid line is the Padé approximant explained in the text.

$$\frac{\sigma}{\sigma_3} = 1 + \frac{3 \left[ (\sigma_1 - \sigma_2)(2\sigma_2 + \sigma_3) + \left( \frac{b+h}{h} \right)^3 (\sigma_1 + 2\sigma_2)(\sigma_2 - \sigma_3) \right] c}{\left[ (\sigma_1 + 2\sigma_2)(\sigma_2 + 2\sigma_3) + 2 \left( \frac{b}{b+h} \right)^3 (\sigma_1 - \sigma_2)(\sigma_2 - \sigma_3) \right] c} + O(c^2) \quad (5)$$

because the parameter  $[(b_i + h)/b_i]^3$  will be different for each particle. Equation 6 for  $n$  different sand particle sizes each with volume fraction  $c_i$  ( $\sum c_i = c$ ) becomes

$$\frac{\sigma}{\sigma_p} = 1 + \sum_{i=1}^n m_i c_i \equiv 1 + \langle m \rangle c + O(c^2) \quad (7)$$

where

$$\langle m \rangle = \frac{\sum_{i=1}^n c_i m_i}{c} \quad (8)$$

Using the sand particle size distribution given in Table 1 by volume, we can find the value of  $m$  for the random mortar model averaged over the appropriately weighted four values of  $b_i$  as in eq 8.

Figure 8 shows a graph of this average slope  $\langle m \rangle$  as a function of  $\sigma_s/\sigma_p$ . Note in the limit of  $\sigma_s/\sigma_p = 1$ , the slope  $\langle m \rangle = -1.5$ , which is the known exact result for insulating spherical inclusions of any size distribution [27]. The marked point on the graph is at  $\sigma_s/\sigma_p = 8.26$ , which is the point at which the slope  $\langle m \rangle = 0$ . At this value, adding a few sand grains would, to leading order in the sand volume fraction, have no effect on the overall conductivity, keeping its value at the bulk cement paste value. In Figure 7, it was found that a value of  $\sigma_s/\sigma_p \approx 8$  was required to make the composite conductivity equal to the bulk cement paste conductivity at a sand volume fraction of 55%. This implies that there is information about the shape of the conductivity versus sand volume fraction curve for this particular sand size distribution and interfacial zone width obtainable without further computation. For  $\sigma_s/\sigma_p \leq 8.26$ , such a curve must start out with negative slope, and  $\sigma/\sigma_p$  will always lie under the bulk cement paste conductivity. For  $\sigma_s/\sigma_p > 8.26$ , the curve will start out with positive slope and always remain above the bulk cement paste conductivity. This cutoff value for the dilute limit slope will of course vary with the sand size distribution. Having larger particles, and keeping the

interfacial zone width the same, will tend to reduce the dilute limit slope at the same value of  $\sigma_s/\sigma_p$ .

Figure 9 shows computed conductivity data for the random mortar model as a function of sand volume fraction for  $\sigma_s/\sigma_p = 20, 5$ , and 1. The sand size distribution was preserved at every volume fraction. The curve for  $\sigma_s/\sigma_p = 20$  is roughly concave up, as the initial slope is greater than 1, and the interfacial zone conductivity is great enough so that the addition of more sand makes this slope even greater. (In principle, the percolation threshold at which the interfacial zone phase becomes continuous might be visible as a fairly sharp break in such a curve. Presumably, the required values of  $\sigma_s/\sigma_p$  are considerably larger than those shown here.) The  $\sigma_s/\sigma_p = 5$  curve has a negative initial slope and remains below 1 as would be expected from the previous predictions. The  $\sigma_s/\sigma_p = 1$  curve roughly follows a  $3/2$  power law in the total cement paste volume fraction, as would be expected because there is no difference between interfacial zone and bulk cement paste in this case.

Using the results of eq 5 for the BCC model implies that the initial slope is zero for  $\sigma_s/\sigma_p = 5.5$ , nearly equal to the value needed to make  $\sigma/\sigma_p = 1$  at 54% sand, so that a fairly similar picture will hold for the ordered model as well.

## Comparison with Experimental Evidence

### Electrical Conductivity

There has been very little experimental work in which both the electrical properties of mortars and the underlying cement paste have been measured. It is hoped

TABLE 1. Sand size distribution used in random mortar model

Diameter ( $\mu\text{m}$ )	Volume Fraction of Total Sand Content
250	0.1895
500	0.2233
750	0.2317
1,500	0.3555

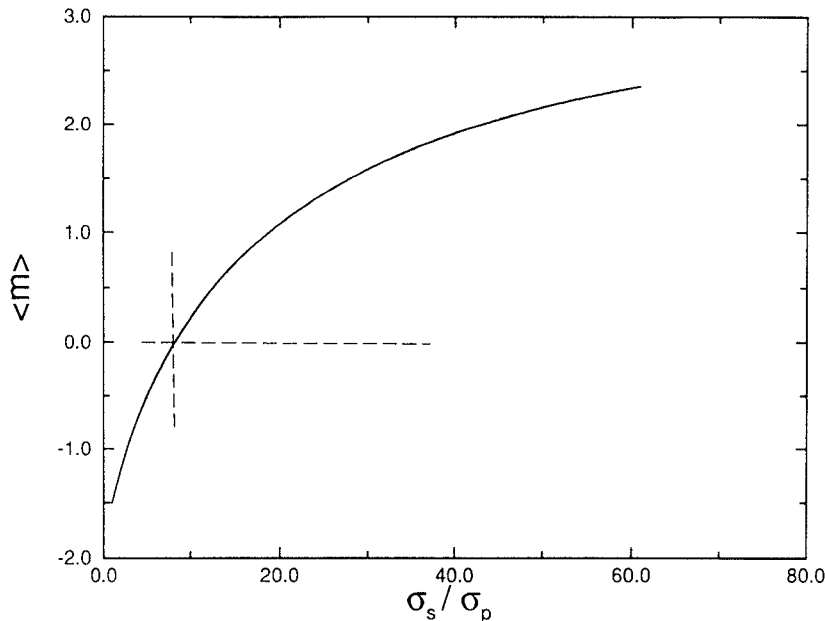


**FIGURE 8.** The exact initial slope of the conductivity, in the limit of dilute sand concentration, is shown as a function of  $\sigma_s/\sigma_p$  for the sand size distribution (see Table 1) of the random mortar model.

that the model presented in this paper will encourage such measurements. However, there are two papers in which measurements of the correct parameters were attempted [10,44].

The first paper [44] contains chloride diffusivity measurements made for cement pastes and mortars with several different sand volume fractions. The ratio of the overall diffusivity to the cement paste diffusivity is, via the Nernst-Einstein relation, the same as the ratio  $\sigma/\sigma_p$  [2]. It was found that this ratio was on the order of 1-2 for both 0.4 and 0.5 w:c mortars at about 50% sand content. Using Figure 7, this result implies, assuming that the sand particle size distribution was similar to that used in our random mortar model, that  $\sigma_s/\sigma_p$  was roughly between 10 and 20, in agreement with the experimental results discussed earlier on flat aggregate interfaces [11,12]. However, another paper that attempted to measure the conductivity of mortar as a function of sand volume fraction found completely different results [10].

Ping and Tang [10] found a roughly linear dependence of mortar conductivity on sand volume fraction, with the slope always negative. They used an approximate formula for the electrical conductivity of the mortar as a function of sand content,  $\sigma_s/\sigma_p$ , and  $h$  to try to extract information about the interfacial zone conductivity. As this formula does not even agree with the exact result for the dilute limit shown in eq 5 and Figure 8, any information obtained by it on the interfacial zone conductivity is suspect [10]. The experimental data also appears to have problems. For quartz aggregate mortars, which almost certainly have high porosity interfacial zones, Ping and Tang find mortar conductivity values that are up to four times lower than

the cement paste values at sand fractions of 50%. This value seems too low, especially when compared to the 3/2 power law [27] that predicts a conductivity,  $(0.5)^{3/2} = 0.35$ , only three times lower than the paste value when the interfacial zone has the same conductivity as the bulk cement paste. In these quartz sand mortars, we expect that the interfacial zone conductivity is indeed greater than the bulk cement paste value, so that overall conductivity should be significantly higher than the 3/2 power law result, not lower.

A possible problem with the experimental data in ref 10 is that a fixed frequency measurement of the conductivity was used. It has been shown that variable frequency AC measurements (impedance spectroscopy) must be used to properly define the DC response of ionic conduction systems like cement paste and mortars [5,45]. Fixed frequency measurements do not necessarily correctly eliminate the effect of the electrode-sample impedance, so that in general too high values of resistance, and therefore erroneously low values of conductivity, will be measured [45].

### Fluid Permeability

It is interesting to try to extend the modeling work to include fluid permeability. However, this can only be done approximately via the following analogy. The correct way to calculate the permeability of a mortar would be to solve the Navier-Stokes equations [46] for the random pore space, which would include bulk cement paste pores as well as interfacial cement paste pores. However, because we are considering mortar at the sub-millimeter scale in this paper, we can use Darcy's law with the appropriate phase permeabilities for the three-component composite: sand ( $K_a$ ), interfacial

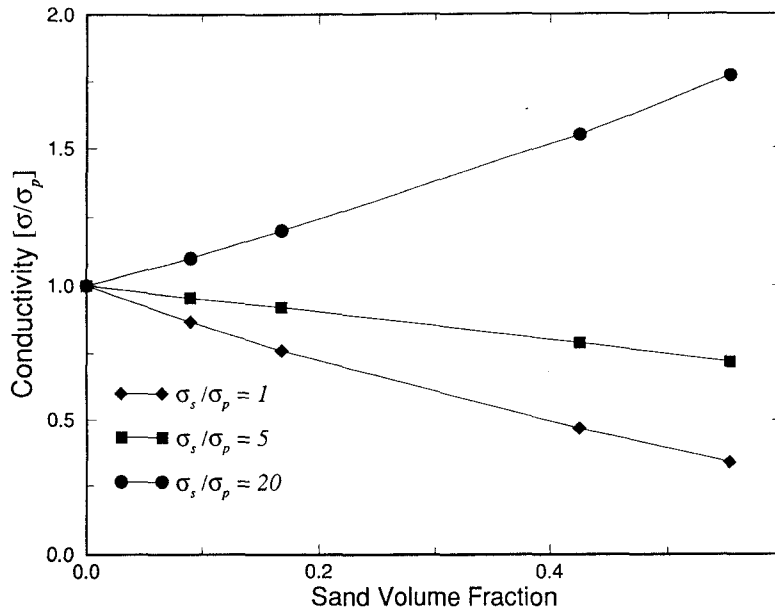


FIGURE 9. Composite conductivities (calculated by random walk simulations) for the random mortar model are shown as a function of sand concentration for several values of the interfacial zone conductivity. (Normalization is as in Figures 6 and 7.)

zone cement paste ( $K_s$ ), and bulk cement paste ( $K_p$ ). Darcy's law for a spatially varying permeability is:

$$\mathbf{v}(\mathbf{r}) = -\frac{K(\mathbf{r})\nabla P(\mathbf{r})}{\eta} \quad (9)$$

where  $\mathbf{v}(\mathbf{r})$  is the fluid velocity,  $K(\mathbf{r})$  is the permeability,  $P(\mathbf{r})$  is the pressure at a position  $\mathbf{r}$ , and  $\eta$  is the fluid viscosity. If we identify  $v(\mathbf{r})$  with  $j(\mathbf{r})$ , the electrical current density,  $K(\mathbf{r})/\eta$  with the electrical conductivity, and  $P(\mathbf{r})$  with the electrical voltage, then this equation is identical with the equation for steady state current flow, with the same boundary conditions, so that all the results we have obtained for electrical conductivity can be reinterpreted for permeability, albeit approximately. (A recent paper has shown that the correct equation to be used in this case is Brinkman's equation but that this use of Darcy's law should be a reasonably good approximation [46].)

If Darcy's law is used, the next question to be raised is: what is the effective value of  $K_s/K_p$ , the key parameter analogous to  $\sigma_s/\sigma_p$ ? One way to estimate this quantity is to make use of the Katz-Thompson (K-T) equation, which predicts the permeability of a porous medium in terms of its conductivity and a critical pore radius characteristic of the largest connected pores in the material defined by a mercury intrusion experiment [1,47]. The K-T equation has recently been shown to work reasonably well on cement based materials [44,48,49], although using conductivities estimated from mercury injection curves did not work as well as directly measured conductivities [50]. The K-T equation also seems to work better for higher water:

cement ratios ( $\geq 0.5$ ) then for lower ones ( $\leq 0.4$ ) [44,48]. Neglecting constants of proportionality, the K-T equation is

$$k \sim \frac{\sigma}{\sigma_0} d^2 \quad (10)$$

where  $\sigma/\sigma_0$  is the conductivity of the porous material relative to the conductivity  $\sigma_0$  of the conductive phase it contains, and  $d$  is the critical pore diameter. If we assume that the value of  $d$  for interfacial zone cement paste is about 10 times as large as that for the bulk cement paste, in rough agreement with the available mercury intrusion evidence [15], and if we take the interfacial zone conductivity to be about 10 times larger than that of the bulk cement paste, in rough agreement with experiments on flat aggregates, then we would expect that the ratio  $K_s/K_p$  would be about 1,000.

The largest value of  $K_s/K_p$  or  $\sigma_s/\sigma_p$  computed in Figure 7 was only 50, but we can use the fitted Padé approximant, which should be more accurate in this limit, to estimate the overall conductivity or permeability to be about 35 times that of the bulk cement paste. Data in ref 44 indicate that the permeabilities of mortars with about 50% sand are about 20 to 60 times higher than the equivalent cement paste mortar, again in rough agreement with the model prediction.

These analyses of the available experimental data in light of the model predictions should serve to motivate more experimental work on mortars with a wide range of sand fractions including the dilute limit of a few percent sand volume fraction. Generally, it appears that impedance spectroscopy should be used to mea-

sure the conductivity, as this is easier than making direct measurements of the diffusivity. Conductivity can then be related to diffusivity via the Nernst-Einstein relation [2].

## Discussion of Future Work

An important goal of future work, based on the techniques and results of this paper, will be to develop a general equation for the conductivity and diffusivity of concrete. The inputs to such an equation would be: (1) the chemistry, water:cement ratio, and degree of hydration of the cement to determine the bulk matrix conductivity; (2) interfacial zone characteristics; (3) aggregate size distribution and volume fraction; and (4) computations like those in this paper. With such an equation, the conductivity and diffusivity of a concrete could be determined with good accuracy at the mix design stage based on fundamental microstructural parameters.

There are two (at least) possible complications in determining the conductivity of mortar or concrete in such a general equation that is not directly addressed by the work covered in this paper. The first is the following. In mortar with a fixed water:cement ratio, the interfacial zone cement paste has less cement and therefore more porosity than would be expected for this water:cement ratio, implying that the bulk cement paste will have slightly more cement and therefore a lower water:cement ratio than the nominal value. The results of ref 15 imply that a typical mortar or concrete has one-fourth to one-third of its cement paste volume in the interfacial region, where the interfacial region is taken to be about 20  $\mu\text{m}$ , the region where most of the larger pores reside. This value implies that there could be a significant effect on the water:cement ratio of the bulk cement paste. This effect would have to be allowed for in a general equation.

The second possible complication is that some kind of assumption about the uniformity of curing must be made, because the local electrical conductivity in a concrete will depend on the local degree of hydration. Water loss at surfaces and self-dessication, among other factors, will effect the uniformity of curing in a typical piece of concrete. A general equation for conductivity, as described previously, must be able to be applied to concrete whose degree of hydration will probably not be uniform.

The same kind of model discussed in this paper can also be used to help understand the role of the interfacial zone on the elastic properties of mortar and concrete. The effect of interfacial zone cement paste on elastic moduli has already been experimentally studied [17]. By holding the aggregate in a mortar at fixed volume fraction but varying the average aggregate size

and thereby the surface area, researchers produced significantly lower elastic moduli [17]. Increasing the aggregate surface area at fixed aggregate volume fraction would certainly increase the volume fraction of interfacial zone cement paste at the expense of bulk cement paste, so that we may conclude that the elastic moduli of interfacial zone cement paste are smaller than those of bulk cement paste, in keeping with a higher interfacial zone porosity. Another recent analysis of elastic moduli led to this same conclusion [18]. It should be possible to carry out computations similar to those described in this paper for the elastic moduli of mortars and to quantitatively understand the effect of the interfacial zone phase on the composite elastic moduli. Work on two-dimensional digital image based models of mortars is currently being carried out on elastic moduli and elastic drying shrinkage [51]. This should give at least qualitative insight into real material behavior at arbitrary sand volume fractions. The dilute limit for the elastic moduli of coated spheres has only very recently been derived [52,53] and will make possible analyses of dilute limit experimental measurements of the elastic moduli. These dilute limit moduli measurements will provide direct measurements of interfacial zone elastic properties.

## Summary

We have shown, assuming a well-defined thickness and conductivity, how the presence of the interfacial zone cement paste influences the overall conductivity of a mortar. Although the aggregate size distribution used was typical of a mortar, the same general behavior is expected of a concrete. Because the interfacial zone cement paste occupies a significant fraction of the total cement paste phase, up to one-fourth or one-third, and because it is percolated, the higher conductivity of this phase in a plain portland cement mortar or concrete will cause the overall conductivity of the mortar or concrete to be higher than that expected for just a simple two-phase (bulk cement paste plus aggregate) composite. Just how much higher is determined by the value of  $\sigma_s/\sigma_p$ , the ratio of the interfacial zone cement paste conductivity to that of the bulk cement paste. For small sand fractions, on the order of 5% or so, the overall conductivity can be predicted analytically for any given sand size distribution, whereas for larger sand volume fractions, numerical computation is necessary. The random walk algorithm discussed in this paper can perform this task accurately.

## Acknowledgments

We are grateful to Daniel Hong for useful conversations concerning the random walk algorithm in two-conducting-phase materials. Part

of this work has been supported by the National Science Foundation through the Science and Technology Center for Advanced Cement Based Materials. LMS thanks the National Institute of Standards and Technology for partial support of his sabbatical leave from Schlumberger.

## References

1. Garboczi, E.J. *Cem. Conc. Res.* **1986**, *20*, 591-601.
2. Atkinson, A.; Nickerson, A.K. *J. Mater. Sci.* **1984**, *19*, 3068-3078.
3. Taylor, H.F.W. *Cement Chemistry*; Academic Press: San Diego, 1990.
4. Garboczi, E.J.; Bentz, D.P. *J. Mater. Sci.* **1992**, *27*, 2083-2092.
5. Coverdale, R.T.; Christensen, B.J.; Mason, T.O.; Jennings, H.M.; Bentz, D.P.; Garboczi, E.J. *J. Mater. Sci.* **1995**, in press.
6. Whittington, H.W.; McCarter, J.; Forde, M.C. *Mag. Conc. Res.* **1981**, *33*, 48-60.
7. Coverdale, R.T.; Christensen, B.J.; Mason, T.O.; Jennings, H.M.; Garboczi, E.J. *J. Mater. Sci.* **1994**, *29*, 4984-4992.
8. Christensen, B.J.; Mason, T.O.; Jennings, H.M.; Bentz, D.P.; Garboczi, E.J. *MRS Soc. Symp. Proc.* **1992**, *245*, 259-264.
9. Olson, R.A.; Christensen, B.J.; Coverdale, R.T.; Ford, S.J.; Jennings, H.M.; Mason, T.O.; Garboczi, E.J. Submitted for publication.
10. Ping, X.; Tang, M. *Il Cemento* **1988**, *85*, 33-41.
11. Ping, X.; Beaudoin, J.J.; Brousseau, R. *Cem. Conc. Res.* **1991**, *21*, 515-522.
12. Bretton, D.; Ollivier, J.-P.; Ballivy, G. In *Interfaces in Cementitious Materials*; Maso, J., Ed.; E. & F.N. Spon: London, 1993; pp 269-278.
13. Garboczi, E.J. *Mater. Struct.* **1993**, *26*, 191-195.
14. Mindess, S.; Young, J.F. *Concrete*; Prentice-Hall: Englewood Cliffs, NJ, 1981.
15. Winslow, D.N.; Cohen, M.; Bentz, D.P.; Snyder, K.A.; Garboczi, E.J. *Cem. Conc. Res.* **1994**, *24*, 25-37.
16. Goldman, A.; Bentur, A. *Cem. Conc. Res.* **1993**, *23*, 962-972.
17. Cohen, M.D.; Goldman, A.; Chen, W.-F. *Cem. Conc. Res.* **1994**, *24*, 95-98.
18. Nilsen, A.U.; Monteiro, P.J.M. *Cem. Conc. Res.* **1993**, *23*, 147-151.
19. Scrivener, K.L. In *Materials Science of Concrete I*; American Ceramic Society: Westerville, OH, 1989.
20. Barnes, B.D.; Diamond, S.; Dolch, W.L. *J. Am. Ceram. Soc.* **1979**, *62*, 21-24.
21. Bentz, D.P.; Garboczi, E.J.; Stutzman, P.E. In *Interfaces in Cementitious Materials*; Maso, J., Ed.; E. & F.N. Spon: London, 1993; pp 107-116.
22. Young, J.F. In *Permeability of Concrete*, ACI SP-108; Whiting, D.; Hall, A., Eds.; American Concrete Institute: Detroit, MI, 1988; pp 1-18.
23. Houst, Y.F.; Sadouki, H.; Wittmann, F.H. In *Interfaces in Cementitious Composites*, Maso, J., Ed.; E. & F.N. Spon: London, 1993; pp 279-288.
24. Bentz, D.P.; Schlangen, E.; Garboczi, E.J. In *Materials Science of Concrete IV*; Skalny, J., Ed.; American Ceramic Society: Westerville, OH, 1995.
25. Rashed, A.I.; Williamson, R.B. *J. Mater. Res.* **1991**, *6*, 2004-2012.
26. Zhang, M.H.; Gjorv, O.E. *Cem. Conc. Res.* **1990**, *20*, 610-618.
27. De La Rue, R.E.; Tobias, C.W. *J. Electrochem. Soc.* **1959**, *106*, 827-833.
28. Bourdette, B.; Ringot, E.; Ollivier, J.-P. Submitted for publication.
29. Halperin, W.P.; Jehng, J.-Y.; Song, Y.-Q. *Mag. Res. Imag.* **1994**, *12*, 169-173.
30. Bhattacharja, S.; Moukwa, M.; D'Orazio, F.; Jehng, J.-Y.; Halperin, W.P. *J. Adv. Cem. Based Mater.* **1993**, *1*, 67-76.
31. Kittel, C. *Introduction to Solid State Physics*, 5th ed.; J. Wiley & Sons: New York, 1976, pp 13-16.
32. Day, A.R.; Garboczi, E.J. To be submitted for publication.
33. Douglas, J.F.; Garboczi, E.J. *Adv. Chem. Phys.* In press.
34. Schwartz, L.M.; Banavar, J.R. *Phys. Rev. B* **1989**, *39*, 11965-11971.
35. Kim, I.C.; Torquato, S. *Phys. Rev. A* **1991**, *43*, 3198-3201.
36. Hong, D.C.; Stanley, H.E.; Conoglio, A.; Bunde, A. *Phys. Rev. B* **1986**, *33*, 4564-4573.
37. Schwartz, L.M.; Garboczi, E.J.; Bentz, D.P. Submitted for publication.
38. Sen, P.N.; Scala, C.; Cohen, M.H. *Geophys.* **1981**, *46*, 781-795.
39. Wong, P.Z. *Phys. Today* **1988**, *41*, 24-35.
40. Bender, C.M.; Orszag, S.A. *Advanced Mathematical Methods for Scientists and Engineers*; McGraw-Hill: New York, 1978.
41. Johnson, D.L.; Plona, T.J.; Kojima, H. In *Physics and Chemistry of Porous Media II (Ridgefield, 1986)*, AIP Conference Proceedings No. 154; Banavar, J.; Koplik, J.; Winkler, K.W., Eds.; American Institute of Physics: New York, 1986; Schwartz, L.M.; Sen, P.N.; Johnson, D.L. *Phys. Rev. B* **1989**, *40*, 2450-2459.
42. Torquato, S. *Appl. Mech. Rev.* **1991**, *44*, 37-76.
43. Hashin, Z. *J. Appl. Mech.* **1983**, *50*, 481-505.
44. Halamickova, P.; Detwiler, R.J.; Bentz, D.P.; Garboczi, E.J. *Cem. Conc. Res.* In press.
45. Christensen, B.J.; Mason, T.O.; Jennings, H.M. *J. Am. Ceram. Soc.* **1992**, *75*, 939-945.
46. Martys, N.; Bentz, D.P.; Garboczi, E.J. *Phys. Fluids A* **1994**, *6*, 1434-1439.
47. Katz, A.J.; Thompson, A.H. *J. Geophys. Res.* **1987**, *92*, 599-607.
48. Christensen, B.J. Ph.D. Thesis; Northwestern University: Evanston, IL, 1993.
49. Christensen, B.J.; Coverdale, R.T.; Olson, R.A.; Ford, S.J.; Garboczi, E.J.; Jennings, H.M.; Mason, T.O. *J. Am. Ceram. Soc.* **1994**, *77*, 2789-2804.
50. El-Dieb, A.; Hooton, R.D. *Cem. Conc. Res.* **1994**, *24*, 443-450.
51. Neubauer, C.M.; Jennings, H.M.; Garboczi, E.J. Submitted for publication.
52. Herve, E.; Zaoui, A. *Int. J. Eng. Sci.* **1993**, *31*, 1-10.
53. Iske, P.L.; Sterk, N.K.J.; Oortwijn, J. *Physica A* **1994**, *209*, 96-128.